Original Article

MOLECULAR METABOLISM

Evaporative cooling provides a major metabolic energy sink

Ildiko Kasza [1], Doug Adler [2], David W. Nelson [3], C.-L. Eric Yen [3], Sabrina Dumas [3], James M. Ntambi [3,4], Ormond A. MacDougald [7], Diego Hernando [5], Warren P. Porter [6], Fred A. Best [2], C.M. Alexander [1,*]

ABSTRACT

Objective: Elimination of food calories as heat could help redress the excess accumulation of metabolic energy exhibited as obesity. Prior studies have focused on the induction of thermogenesis in beige and brown adipose tissues as the application of this principle, particularly because the β-adrenergic environment associated with thermogenic activation has been shown to have positive health implications. The counterpoint to this strategy is the regulation of heat loss; we propose that mammals with inefficient heat conservation will require more thermogenesis to maintain body temperature.

Methods: Surface temperature thermography and rates of trans-epidermal water loss were integrated to profile the total heat transfer of genetically-engineered and genetically variable mice.

Results: These data were incorporated with energy expenditure data to generate a biophysical profile to test the significance of increased rates of evaporative cooling.

Conclusions: We show that mouse skins vary considerably in their heat retention properties, whether because of naturally occurring variation (SKH-1 mice), or genetic modification of the heat-retaining lipid lamellae (SCD1, DGAT1 or Agouti A^y obese mice). In particular, we turn attention to widely different rates of evaporative cooling as the result of trans-epidermal water loss; higher rates of heat loss by evaporative cooling leads to increased demand for thermogenesis. We speculate that this physiology could be harnessed to create an energy sink to assist with strategies aimed at treating metabolic diseases.

Keywords Trans-epidermal water loss; Evaporative cooling; Epidermal barrier; Syndecan-1; Obesity; Mouse skin; Thermogenesis; Dermal white adipose tissue; Energy expenditure; Brown adipose tissue

1. INTRODUCTION

Heat generation (thermogenesis) could potentially be harnessed by human subjects to consume calories and prevent obesity [4,10,16,20]; furthermore, it has been shown that activated thermogenic tissues may have signaling functions in mammals that promote metabolic health and prevent disease [3,20]. However, if a thermogenic strategy is to be effectively harnessed to improve health, sources of heat loss are equally important to understand. Here, we focus on how heat is lost through mammalian skins, with the ultimate goal of modifying skin properties to impact thermogenesis and health.

Like breathable synthetic materials (such as GORE-TEX™), skin is a permeability barrier organized into a series of lamellae, each with different functions and properties [31]. In particular, water proofing and breathability are governed by two lipid bio-membranes (Figure 1A). One is associated with the extracellular complex lipid mixtures produced by epidermal keratinocytes and sebocytes, consisting of approximately 50% ceramides, 25% cholesterol, and 15% long and very-long chain fatty acids, together called the epidermal barrier [28]. The other is associated with a contiguous layer of adipocytes underneath the connective tissue of the dermal layer, called the dermal white adipose tissue (dWAT) in mice and subcutaneous white adipose tissue (scWAT) in humans [1].

Typically, we focus on water loss through perspiration as a cooling mechanism for over-heated mammalian bodies. However, even at environmental temperatures less than body temperature (sub-thermoneutral), it is well-established that mammals have a considerable and constitutive rate of trans-epidermal water loss (TEWL). Rate of water loss for any given individual depends upon their genetics, time of day, and states of inflammation and disease [8,15,36,37]. In extreme conditions of skin loss or dysfunction, high rates of water loss are associated with dehydration stress, for example in burn victims.

Skin has been highlighted as the main effector of obesity-and diabetes-related phenotypes by several studies of enzymes important to lipid metabolism in mice [28]. Thus knockouts of genes encoding enzymes such as ACBP1, SCD1, and DGAT1 change skin permeability,

[1]McArdle Laboratory for Cancer Research, University of Wisconsin-Madison, United States [2]Space Science and Engineering Center, University of Wisconsin-Madison, United States [3]Department of Nutritional Sciences, University of Wisconsin-Madison, United States [4]Department of Biochemistry, University of Wisconsin-Madison, United States [5]Department of Radiology, University of Wisconsin-Madison, United States [6]Department of Zoology, University of Wisconsin-Madison, United States [7]Department of Molecular and Integrative Physiology, University of Michigan, United States

*Corresponding author. E-mail: cmalexander@wisc.edu (C.M. Alexander).

Received April 11, 2019 • Revision received June 8, 2019 • Accepted June 27, 2019 • Available online 1 July 2019

https://doi.org/10.1016/j.molmet.2019.06.023

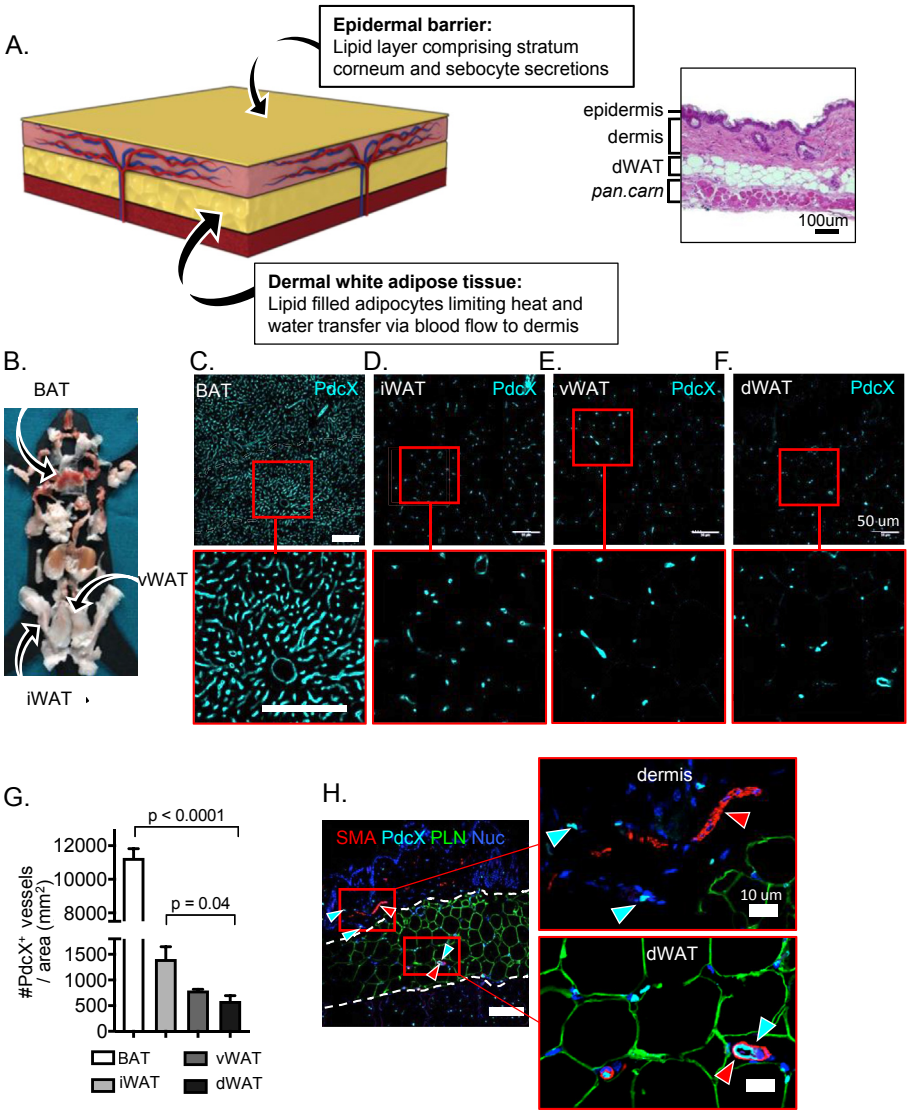

Figure 1: The structure of mouse skin. **A**. A scheme of skin structure illustrates two lipid bio-membranes, colored in yellow. The outer bio-membrane of the ceramide-enriched epidermis is the water-proofing component of skin: ceramide-based lipids of the stratum corneum generate a highly ordered gel phase membrane with restricted mobility, called the epidermal barrier [31]. Junctions between keratinocytes and regulated water flow through aquaporins comprise a key "active" component of the epidermal barrier, reactive on acute time scales; on a slower time scale (days), the lipid composition of the stratum corneum changes as the superficial layers are sloughed and renewed [36]. The thickness of the dermal white adipose tissue (dWAT) is regulated by interaction with microbes, ambient temperature and the stage of the hair cycle, and by genetics, diet and sex [1,2]. In between lies the dermis, laced with two vascular beds to allow adjustable blood volumes to control heat loss. At the right, for comparison, an H&E stained cross section of mouse skin (*panniculus carnosus* muscle layer; *pan carn*). Four adipose depots with different functions were collected for evaluation of vascular density (sites of each depot shown on left; **B**); dWAT, inguinal ("subcutaneous") white adipose tissue (iWAT), brown adipose tissue (BAT) and visceral white adipose tissue (vWAT). Sections of each type were stained for podocalyxin, a vascular-associated antigen (**C**–**F**), and the density of vessels quantified (**G**). Sections of each were also stained with smooth muscle actin (SMA) to reveal pericyte-supported blood vessels, perilipin (PLN) to outline adipocytes and DAPI (Nuc) to counter-stain nuclei (**H**). The scale bar shown is 50 μM and applies to all panels C-F.

and are sufficient to confer metabolic phenotypes [28,39,41,43,46]. Surprisingly, specific targeting of the SCD1 mutation to skin (so-called **SKO** mice) showed that this was enough to confer resistance to diet-induced obesity [41]. Indeed, skin has been proposed to be both sensory and reactive to many metabolic and environmental cues [13]. With that in mind, here we calculate the energy dissipation created by evaporative cooling through the bilaminar semi-permeant membranes of mouse skin and show that increased rates of evaporative cooling partly, or completely, account for increased energy expenditure reported in mouse strains with deficient lipid layers. Vice versa, we show that obese mice show lower trans-epidermal water loss. This raises the interesting possibility that evaporative cooling could be a significant player in establishing the metabolic budget and could be manipulated to consume calories and engage the health-promoting aspects of thermogenesis.

2. RESULTS

2.1. Histological analysis of blood vessel pattern in specific adipose depots

Skin regulates the loss of heat from the body, most efficiently via dissipation of heat from internal organs through blood flow. To assess the delivery pattern for blood to the skin, we evaluated skin sections by immunohistochemical staining for podocalyxin (**PdcX**) and smooth

muscle actin (**SMA**) and compared the distribution and size of blood vessels with other fat depots. Anti-PdcX antibodies stain all endothelial (and lymphoid) vessels, irrespective of size, and antibodies against smooth muscle actin (SMA) reveal contractile blood vessels. We found that, of the four categories of fat examined, the density of blood vessels was lowest in dWAT (Figure 1B—G). The most vascularized fat (brown adipose tissue, BAT; specialized for the dissemination of mitochondrial-derived heat) shows a blood vessel density of 11,000/mm^2 compared to dWAT (500/mm^2). Futile biochemical cycles can be activated in subcutaneous "beige" white adipose tissue (inguinal WAT; iWAT) to serve a heating function [27]; these tissues also have a higher vascular density (3-fold) than dWAT.

The small capillary beds that deliver oxygen to dWAT are not SMA positive (Figure 1H). In contrast, there are few, large "perforator" pericyte-lined blood vessels coming from the body interior, through the muscle/mesothelial skin lining and into the dermis. These large vessels are evidently contractile, able to vasodilate or contract to regulate the delivery of blood to the outer shell of the skin. We conclude that dWAT comprises the first barrier to heat dissipation from the body core; it is perforated with only sparse delivery points for warm blood to the outermost shell of the dermis. These perforator vessels can be reduced in diameter when mammals are exposed to cool temperatures below sub-thermoneutrality; thus, heat transfer is prevented firstly by dWAT and then by the epidermal barrier.

2.2. Illustration of the paradoxes introduced by assay of surface temperatures

Potential biophysical processes associated with heat transfer from skin are illustrated in Figure 2A; these are convection (heat loss via air, **Qcon**), radiation (heat loss to surroundings via radiation, **Qrad**), and transpiration (water phase change (evaporation) and mass transfer via air, **Qevap**). Conduction (direct contact with objects) is not considered here, as mice tend to avoid contact with conductive surfaces like metal, preferring instead bedding materials with insulating properties. The convective boundary layer barrier at the skin-air interface greatly limits conductive and convective heat loss. Theoretical modeling suggests that this boundary layer effect will overwhelm the potential impact of a thick or thin dWAT layer on passive insulation, which was implied from experimental data by Kasza et al. [25].

To address this issue, we assessed surface temperatures of mouse skins using infrared thermography (forward-looking infrared, FLIR™). Surface temperatures of live mice cannot be used directly to measure heat transfer properties of skins, since heat production is titrated to maintain body temperature homeostasis [34]. In other words, heat production is increased to offset losses and maintain body temperature. To determine the intrinsic biophysical properties of mouse skins, we chose instead to compare properties of pelts from freshly euthanized mice in carefully controlled environmental conditions, laid over a constant 37 °C body temperature-equivalent warm block. We then assayed the surface temperatures using FLIR to assess the insulating properties of samples. We noted discrepancies between measurements performed on wet and dry warm blocks, suggesting that evaporation from the skin surface could be a significant contributor to heat loss.

For example, Figure 2B shows four skins, two genetically modified (SKO and obese/Agouti a/A^y) and two matched control mice, assayed using FLIR on dry and wet blocks. These mouse strains are described and defined in Table 1. On a dry block, evaporative losses are minimized; resistance to heat transfer through thicker skins is revealed by lower surface temperature (Figure 2B), quantified as the difference between the skin surface and the heat block temperature, [T0—T1]. On a "wet block", another effect comes into play; skin is a barrier to evaporative cooling, so the skin surface temperature [T3] is higher than the uncovered wet tissue surface [T2] (Figure 2C). When the same skins assayed in (B) are moved to the wet block, the FLIR image reveals differences in the relative properties of the test skins: thus, despite the fact that skin from SKO mice is thick, it appears cooler than the corresponding thick obese (A^y) skin.

SKO mice carry an epidermal-specific mutation of the lipid metabolizing enzyme, SCD1 (see Table 1). To investigate the discrepancy of surface temperatures described, we considered prior studies of mice with global mutation of the SCD1 locus. These mice show high rates of water transpiration, elevated energy expenditure and cold sensitivity [6]. High rates of evaporative cooling are predicted to lead to cooler surface temperatures. Therefore, we measured the trans-epidermal water loss (TEWL; Figure 2D) of the skins shown in Figure 2B, and illustrated a 3-fold difference in TEWL between SKO and obese (Ay) skins, despite their similar thickness. Indeed, the rate of evaporative cooling, together with resistance to heat transfer by radiative losses, combine to drop the skin surface temperature of SKO skins even lower than the wet tissue background. In contrast, skin from obese (A^y) mice is thick, but does not permit water loss; these two effects offset one another to generate a surface temperature closer to control skins. We chose to focus on heat dissipation through skin by evaporative cooling, using TEWL as an assay.

2.3. Assay of heat transfer by evaporative cooling

To evaluate whether the assay of trans-epidermal water loss from pelts collected after mouse euthanasia could reliably assess water loss rates from mice *in vivo*, we measured TEWL of live mice and then again after euthanasia. We selected four different types of pelt for further investigation (their properties are detailed in Table 1). We sought first to compare TEWL readings from live mice and from mice shortly after euthanasia. For mice with a range of skin types, results were similar for live mice compared to their skins *ex vivo*, laid out on test blocks (Figure 3A). This match was remarkable given the inaccuracies of measuring non-anesthetized mouse subjects (anesthesia changes body temperature rapidly). To decrease the variability associated with live measurements, we used only pelt measurements for further analysis. However, note the caveats of directly extrapolating results to live mice: skin is not typically exposed to water-saturated body tissue *in vivo*, and pelt assay does not include any heat dissemination from circulating blood.

Typically, skin permeability assays are calibrated using positive controls such as acetone extraction or tape-stripping [21]. By way of illustration of the importance of the epidermal lipid barrier to water retention [31], we measured TEWL after an acetone wipe; this treatment increased water transpiration in our assay, in this case approximately 4-fold (Figure 3B).

We conclude that since infrared thermography measures the surface temperature of objects, it represents the sum of two complex and opposing metabolic effectors: surface temperature is decreased by evaporative cooling, but also decreased by insulating biomaterials. Physiologically, evaporative cooling represents an energy loss, whereas insulation reflects heat conservation (at sub-thermoneutral temperatures). Metabolically, these two functional attributes of skin have an opposite impact on calorie disposition, one spends calories, the other conserves them. Surface temperature alone is therefore not a reliable readout of the metabolic properties of skin; the assay of transpiration rates becomes key.

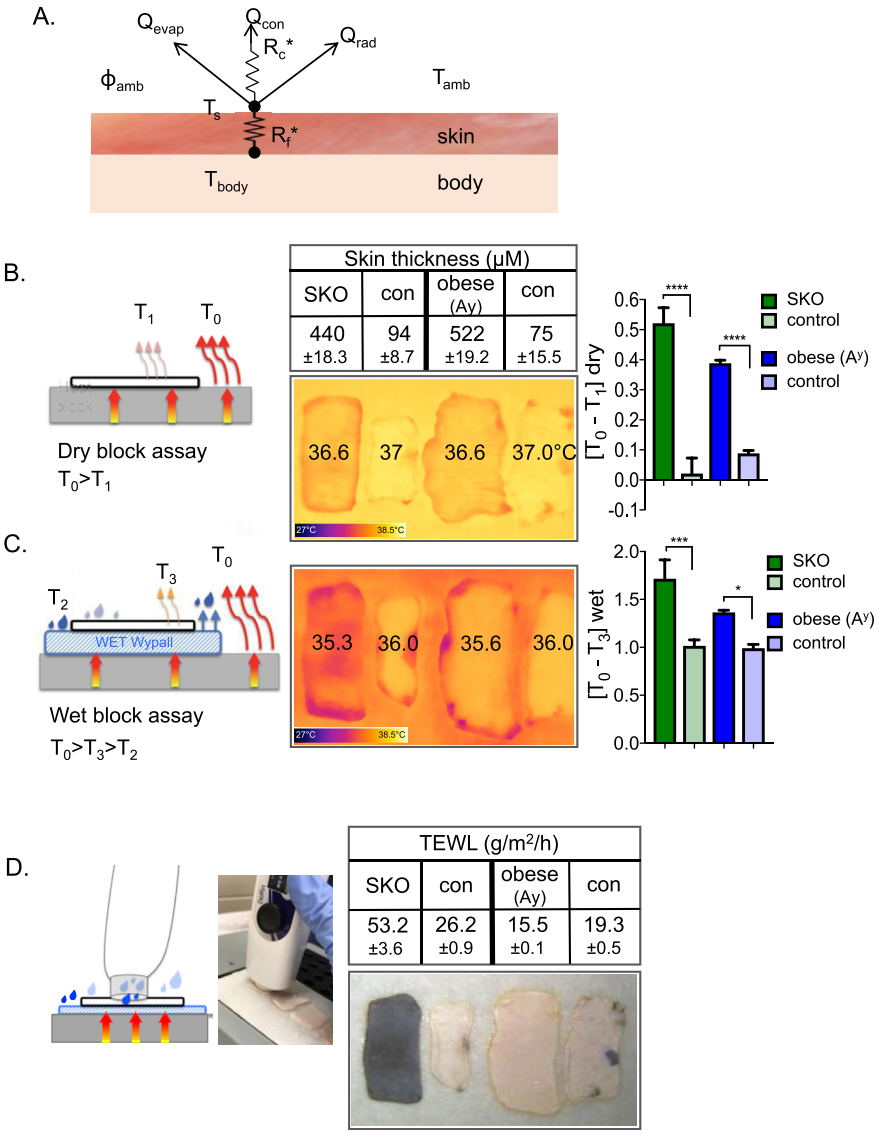

Figure 2: Illustration of the impact of evaporative cooling on heat transfer. **A. Scheme of potential modes of heat loss.** Loss of heat from body temperature (Tbody) to the outside (Tamb) is governed by at least three mechanisms that relate to the resistance of the skin biofabric (described by a factor, Rf) and the biophysical properties of the boundary layer (described by another factor, Rc). Heat can be lost by conduction (Qcon), radiation (Qrad) or evaporation (Qevap); together, these determine the surface temperature (Ts). The rate of radiation is controlled by the gradient of temperature from body to environment (Tamb); conduction by contact surfaces, and evaporative cooling by ambient humidity (ϕamb). **B. Dry block assay.** Skins were excised from mice, transferred to a heat block (**37°C**), and promptly imaged using infrared thermography (FLIR). Skin thickness was measured by histological analysis of sections. Impeded heat flow was visualized as a lower surface temperature (color scale shown at foot of image), and quantified as [T0-T1]dry, where higher values show higher insulation. **C. Wet block assay.** Skins were transferred to a water-saturated tissue substrate (emissivity >0.98, homogeneous background; 37 °C), and imaged by FLIR. The surface temperature recorded is lower for skins with high rates of transpiration and also lower for skins with more insulation (opposing metabolic effects). The surface temperature is quantified as [T0-T3]wet, where values combine these two distinct aspects of skin physiology. **D. Trans-epidermal water loss assay reveals basis for discrepant dry and wet block images**. TEWL was measured using a closed-chamber instrument; results for these skins varied over 3-fold, from skins ranging in thickness by nearly 6-fold (75 and 522 μM). Note that SKO skins appear black due to trapped hair follicles (see detailed descriptions in legend to Figure 4). Thermographic images were analyzed using the FLIR camera software as per Materials and Methods section; shown are mean values ± SEM, analyzed by unpaired 2-tailed *t* tests (****$P < 0.0001$; ***$P < 0.001$; *$P < 0.05$).

2.4. Assay of rates of evaporative cooling in genetically modified mice

We expanded the study to compare various mouse strains with known alterations of the lipid-based skin bio-membranes, two strains with deficient epidermal barriers (DGAT1 KO and SKO) and two with altered dWAT thickness (one thick (A^y), one thin (Sdc1KO)). The reported phenotypes of each genetic modification are summarized along with their impact on energy expenditure (Table 1). For each type of skin, we measured skin permeability, alongside the surface temperatures of skins, loaded onto dry and wet blocks (Figures 4 and 5).

DGAT1 KO mice have a dramatically increased rate of TEWL (50%), compared to control skins (Figure 4A,B, corresponding surface temperatures are shown in Figure 5A). An even higher rate of TEWL is noted in the SKO mice, where it is increased by 100% over control skins (Figure 4C,D; FLIR images in Figure 5B). Note that, as previously reported for mice with the spontaneous SCD1 mutant allele $Scd1^{ab2J}$,

Table 1 — Properties of genetically modified mice used for comparison. Two mouse strains with deficient epidermal lipid barrier function and two with altered thickness of dWAT were evaluated by FLIR and TEWL. The epidermal lipid lamella has been described in detail [28,31,36]; dWAT was introduced in this role more recently [1]. Note that not all mice were evaluated for the phenotypes noted.

Gene	Function of enzyme/protein	Phenotype	Energy expenditure	References
DGAT1 C57BL6	**Diacylglycerol O-acyltransferase.** Important for synthesis of corneocyte permeability barrier	Knockout mouse has alopecia, decreased water repulsion, sebocyte atrophy, low wax di-esters on fur. DGAT2 mutations are much more severe (lethal)	Decreased adiposity, resistant to diet-induced obesity, increased energy expenditure, hyperphagia, impaired thermoregulation leading to torpor during fasting, increased water consumption	[12,47,53]
SKO C57BL6	**Stearoyl-CoA desaturase.** Conversion of saturated to Δ9 unsaturated fatty acids. Important step in triglyceride synthesis	Skin-specific knockout of SCD1 (Keratin14-cre; SCD1 *fl/fl*: SKO) has alopecia, sebocyte atrophy, low wax di-esters on fur.	Resistance to diet-induced obesity, glucose intolerance, and hepatic steatosis. Prone to hyperphagia, increased energy expenditure, cold sensitivity	[41,43]
a/A^{y} Agouti lethal yellow C57BL6	**Gain of function for Agouti peptide.** Antagonist of hypothalamic MC4R	Spontaneously obese. dWAT is increased by 4-fold—400 μM thick. Tumor susceptible.	Hyperphagia, hypoactivity and increased fat mass, insulin-resistant and diabetic.	[40,54]
Sdc1KO BALB/cJ	**Syndecan-1.** Heparan sulfate proteoglycan with many binding activities for growth factors and matrix	Smaller (12%). Layer of dWAT is thin (depleted by 80%). Tumor resistant.	Susceptibility to torpor during fasting, super-activation of thermogenesis, increased energy expenditure	[24,25]

SKO mice have thick skins with no visible sebaceous glands and are dark because of black follicles trapped in the dermis [50,51]. For mice with mutations that affect the dWAT layer, the changes observed followed our prediction. Thus, mice with thin dWAT (Sdc1KO mice) show higher rates of TEWL (increased by 50%; Figure 4E,F and Figure 5C). In contrast, obese A^{y} mice have thick, insulating skins (Figure 4E,F and Figure 5D) with rates of water transpiration decreased by 27%.

2.5. Evaporative cooling is increased for furry skins

Unlike human skin, most mouse skin is furry. We assayed furry skins and were surprised to find that water loss from furry skin was higher than from depilated pelts (Figure 6A,B). We conclude that although fur is a good insulator, it enhances evaporative cooling, by approximately 2-fold, presumably because fur increases the evaporative surface for water loss. Under low humidity conditions, we therefore predict that the insulator properties of fur will diminish.

2.6. More permeable skins are linked to higher thermogenic activation in a genetically variable, outbred mouse strain

Our model predicts that increased evaporative cooling will generate a demand for thermogenesis. We used the natural variation endemic to the SKH1 outbred mouse strain to test for a relationship between TEWL and BAT activation. This mouse strain is hairless (due to a mutation of the Hairless (Hr) gene) but immunocompetent; it is frequently used for dermatological studies due to known parallels with human skin biology [5]. Given that these mice are hairless, we predicted they would be more cold-stressed than hairy counterparts, requiring a higher ambient temperature to be thermoneutral [38,48]; thus 28—32 °C is typically the zone of thermoneutrality for furry mice, and the thermoneutral threshold is shifted upwards for Nude or shaved mice. Assay of SKH1 mice in metabolic cages showed their EE was lower at 35 °C than 31 °C (Figure 7A), confirming that albeit warm, 31 °C housing temperature was still below thermoneutrality for this strain. Food intake was also reduced further at 35 °C, and water consumption increased (Fig. S1A). We were surprised to observe that the TEWL of pelts from mice housed at higher ambient temperature was lower (Figure 7B). Notice the humidity inside metabolic cages is much higher than typical housing conditions; it is determined by the humidity, size of cage, and rate of intake of air for the metabolic cage rig. For these experiments, humidity was measured at 53%, compared to a more standard 20% relative humidity (depending upon the time of year). SKH1 mice showed typical patterns of circadian energy expenditure. When compared to a furry strain (BALB/cJ), their energy expenditure was similar; however, their respiratory calorie source was strongly skewed towards fat utilization (RER; Fig. S1B) SKH1 mice housed at 31 °C showed a depressed body temperature (>1 °C lower, approximately 37 °C) compared to mice housed at room temperature (Figure 7C); this was also observed in mice housed at presumptive thermoneutrality, 35 °C. We used this and other observations to select 31 °C as a suitable threshold temperature to test for a correlation between TEWL and EE. Assay of % body fat, lean body weight, EE, body temperature, food intake, and TEWL showed that these factors varied substantially from mouse to mouse, allowing us to test for correlations (Fig. S1C).

BAT activation is known to associate with at least three parameters, namely 1) higher amounts of the UCP1 protein, assayed by western blots; 2) depleted lipid stores (assayed from histological images) [25]; and 3) higher BAT temperatures, measured by FLIR of live mice [17]. Assay of lipid content of BAT from mice housed at 24, 31 and 35 °C showed that at room temperature, BAT lipid stores were almost entirely depleted for SKH1 mice (Figure 7D). This is consistent with the anticipated cold stress experienced by hairless mice compared to furry mice (compare this level of depletion with those reported for BALB/cJ Sdc1 KO mice [25]).

To screen for BAT activation in live mice, we took FLIR pictures of live mice at various ambient temperatures, with constant 20% humidity. As shown by other studies, the interscapular skin overlaying the BAT depots showed the highest surface temperature body-wide (Figure 8A). The basal BAT temperature of live mice was highest in the coolest housing temperature (ambient temperature of 25 °C; 38.86 ± 0.18 °C), decreasing to 38.46 ± 0.06 °C in warmer housing conditions (31 °C; Figure 8A). Switching the mice from 31 °C housing to 24 °C for 10 min induced a reproducible increase of BAT temperature by 0.81 °C. A side view of mice responding to this cool stress showed that heat was circulating to, or being made by, other tissues, perhaps including heart, liver, or inguinal white adipose tissue [29,45]. Superficial temperatures at these other sites could be as high as interscapular high temperature (but did not exceed it). Thus this non-invasive assay of live hairless mice can be used to assess BAT

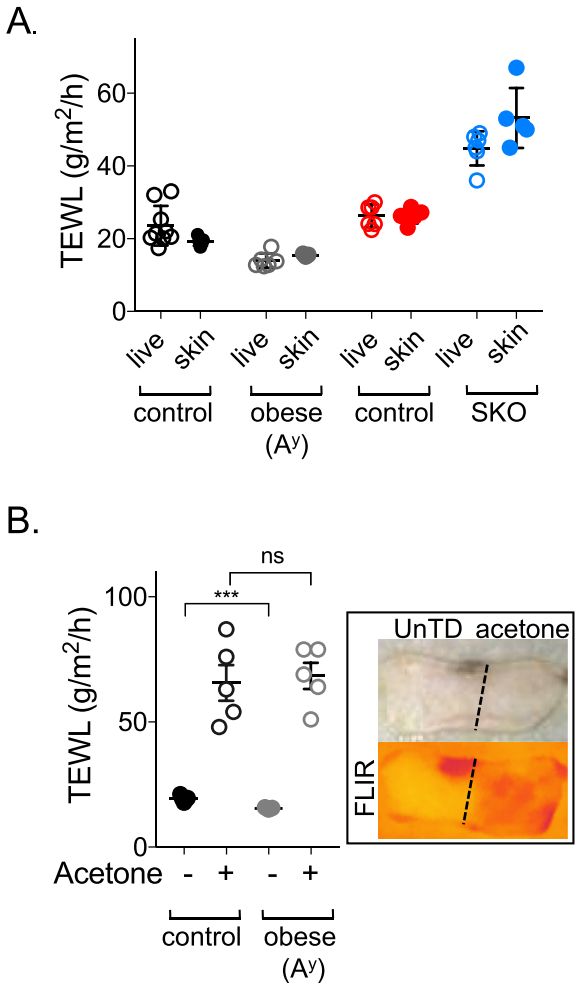

Figure 3: Calibrating the TEWL assay. **A**. Trans-epidermal water loss was compared for the skin of live mice, versus their pelts after euthanasia, for two types of mice included in this study and their respective controls, obese (Ay) and SKO (SCD1 skin specific knockout). **B**. Skins of control and obese mice were wiped with acetone to extract the lipid from the epidermal barrier, by way of positive control for the TEWL assay. Increased evaporative cooling is also visualized as a lower surface temperature assessed by infrared thermography for control mice (FLIR; right hand side). The acetone extraction protocol does not affect dWAT (confirmed by histological analysis of skins after treatment, data not shown). Data are expressed as mean ± SEM. Statistical analysis was performed with unpaired 2-tailed *t* test (***$P < 0.001$, ns = not significant).

activation; however taking pictures of mice gently handled every 10 min produces a longer-term elevation of BAT temperature, indicating their stress response to handling (data not shown).
Skin permeability was measured for mouse pelts using TEWL, and the degree of activation of BAT was assessed by all three criteria of BAT activation (Figure 8B–D). Mice with high TEWL showed significantly higher UCP1 expression (Figure 8B) and lower lipid droplet stores (Figure 8C). There was a trend towards increasing BAT activation measured by the live FLIR assay, with higher rates of evaporative cooling (Figure 8D). This result encouraged us to calculate the impact of increased evaporative cooling rates on the energetics of mouse metabolism.

2.7. Heat flux calculations illustrate the energy drain represented by evaporative cooling

We converted the heat associated with water lost to evaporation into energy as follows:

The rate of energy dissipation associated with evaporation, power [P_{EC}] (J/s or W) = TEWL (g/m^2/s) * surface area of mouse (m^2) * heat of vaporization of water (J/g).
The following assumptions and conversions apply:

- TEWL readings are read in g/m^2/h and are converted to seconds (/3600) for this calculation.
- The heat of vaporization of water = 2400 J/g (calculated for approximate mouse body temp, 37 °C).
- Surface area is calculated for an average mouse and should be re-calculated for experimental subjects that deviate from normal size. Surface area used for these calculations (unless otherwise indicated) was 105 cm^2, to include the evaporative surface area provided by tail, limbs and ear appendages.
- TEWL of the pelt is assumed to be equal across the body surface, despite the lack of fur on appendages and the differences of blood flow in these areas.
- No account is taken of respiratory water losses.

In summary,

Power of evaporative cooling (W/mouse) = TEWL (g/m^2/h)*0.0105 (surface area/m^2)*2400 (J/g)/3600 (s/h) = **TEWL (g/m^2/h) x 0.007**.

By way of example, an increase of TEWL by 20 g/m^2/h converts to an additional energy loss of 0.14 W.
To test the potential significance of this energy sink, we calculated the total power expended by mice, converting the usual energy expenditure assays (kcal/h/kg) to Watts. Indirect calorimetry is often used to assess changes of energy expenditure; the respiratory load is indexed by the consumption of O_2 and production of CO_2 using the Weir equation. To convert the energy expenditure reported in kcal/h/kg to energy (W),

EE [W] = EE [kcal/h/kg]*mass [kg]/0.86 [kcal/h/W].

A comparison of the energy sink associated with evaporative cooling shows that it comprises a significant fraction of total energy expended by a mouse (Table 2 and Figure 10) and broadly correlates with the changes of energy expenditure (either up or down) noted for each genetically manipulated mouse compared to its control.

3. DISCUSSION

3.1. Is evaporative cooling a useful indicator of a metabolic flux that determines susceptibility to obesity?

We have shown that evaporative cooling at the body surface creates a metabolic sink that can account for a significant fraction of total energy metabolism. Strains with known deficiencies in their epidermal lipid barrier have higher evaporative cooling (SKO and DGAT1 KO mice); these strains are already known to be resistant to diet-induced obesity [28]. Indeed, studies from the Ntambi lab revealed the surprising result that the tissue responsible for conferring resistance to diet-induced obesity was the skin of SCD1 mutant mice (SKO), rather than the tissues more typically associated with mis-regulated fat accumulation, like adipose, liver, or gut [42]. Note that SKO mice are resistant to becoming obese, regardless of their dramatic increase of food consumption (100% increase; see Table 2). SCD1 mutant mice showed depleted cutaneous lipids (wax di-esters reduced by 84% and triglycerides are reduced by 72%, along with almost all Δ9 unsaturated fatty acids) [43].

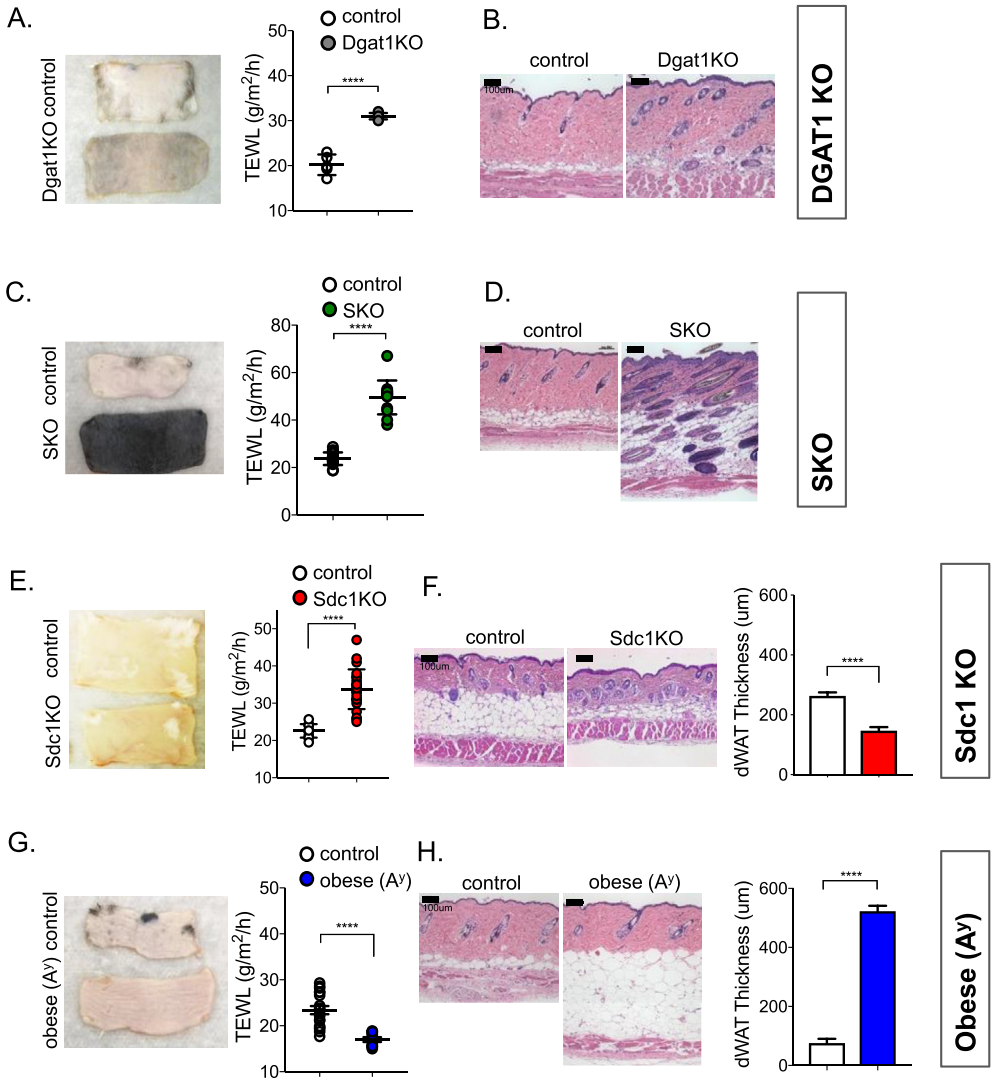

Figure 4: Properties of skins from mice with deficient skin-associated lipid barriers. Skins from DGAT1 KO mice were assayed by TEWL (n = 3; **A**) and by histological analysis (**B**). Skins from skin-specific SCD1 mutant mice (SKO) were assayed by TEWL (n = 3; **C**) and by histological means (**D**). Note the unusual structure of skin from SKO mouse was also observed in a spontaneous mutant strain of the SCD1 allele arising on the DBA/1LacJ background, described by Sundberg et al. [50]. This includes extreme sebaceous gland hypoplasia and abnormally long anagen follicles that are retained deep in the dermis, giving the skin a black color. Skins from Sdc1 KO mice were assayed by TEWL (n = 3; **E**), and by histological analysis (**F**), revealing the depleted dWAT layer (50% thinner). Skins from obese A^y mice were analyzed similarly, by TEWL assay (n = 3; **G**), and histological assay, showing accumulation of dWAT (>400 nm thick; **H**). Data are expressed as mean ± SEM. Statistical analysis was performed with unpaired 2-tailed *t* test (****$P < 0.0001$).

We speculate that the energetic load imposed by increased evaporative cooling may help to prevent obesity in these mouse strains. Activation of thermogenesis induces a wide-ranging systemic change known as the β-adrenergic environment, associated not only with circulating β-adrenergic agonists, but mobilized lipids from several fat depots and other cytokines from integrated organ responses. Accumulating literature suggests that increased exposure of mammals to the β-adrenergic environment is associated with better health in general [20]. Therefore, understanding the factors that control the magnitude and/or duration of this response could provide a natural inexpensive intervention with potentially high impact.

3.2. Calculating energy debts incurred by evaporative cooling

A summary diagram of a typical energy balance is shown in Figure 9, placing thermogenesis in context with other metabolic expenses. Diagrams presented in Figure 10 build on this scheme for the four test strains, summarizing conclusions made by this study (data is drawn from Table 2; Table S1 presents detailed calculations). Table 2 tracks the change in energy in (food consumed), rate of oxidation of calories (energy expenditure) and heat produced in test strains. Chemical energy in = mechanical work done + anabolic rate (chemical energy trapped) + heat produced.

For Sdc1KO mice (thin dWAT), increased evaporative cooling accounts for the increased metabolic rate. Although these mice are susceptible to cold- and fasting-induced torpor, they are also highly tumor-resistant [25,33]. Whether this dramatic cancer-related phenotype is related to their altered energetics remains to be tested. Syndecan-1 is a heparan sulfate proteoglycan with a role in the uptake of lipoprotein particles (at least for liver [49]); it has been shown to be important for maintaining the intestinal epithelial barrier, another barrier between the body and the

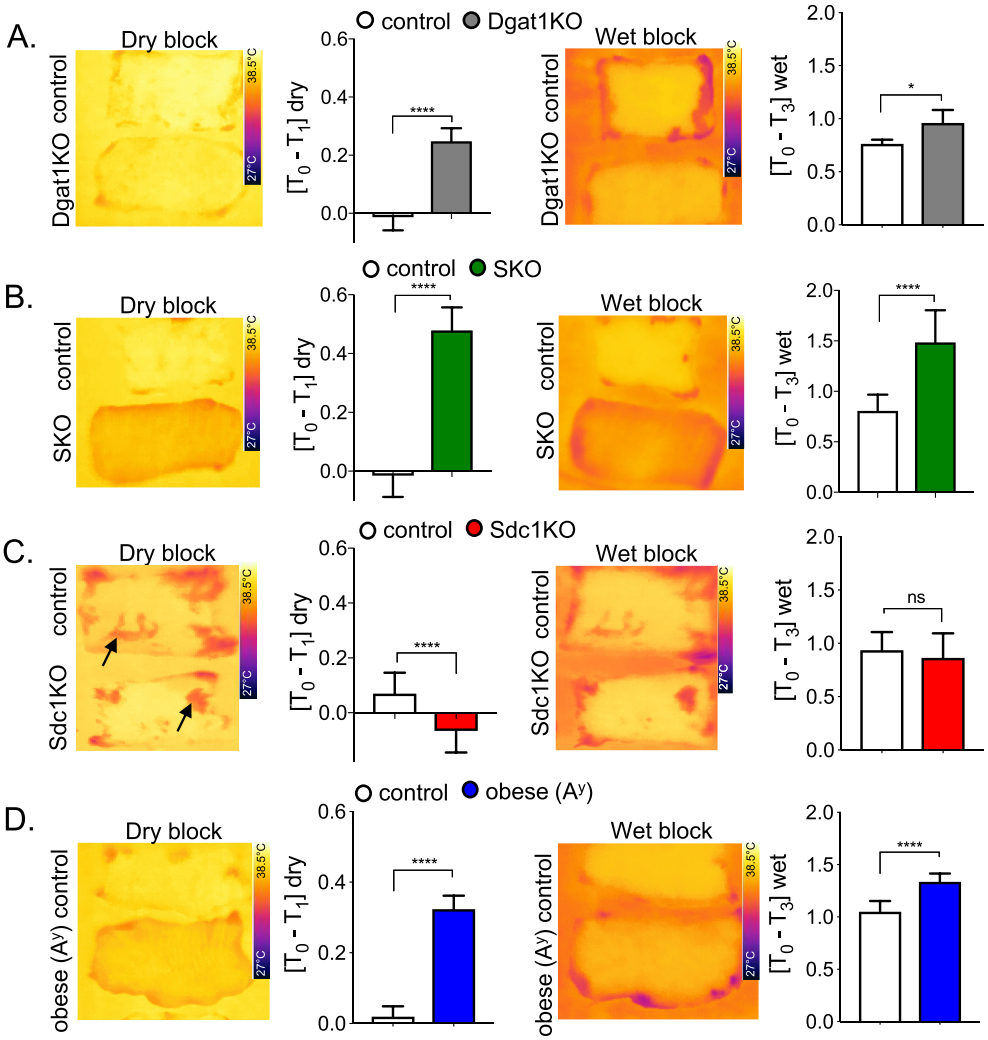

Figure 5: Surface temperature assays of skins from mice with deficient skin-associated lipid barriers. FLIR imaging of skins on dry and wet blocks and quantitation of each assay is shown: When [T0-T1] is positive, skin surface is cooler than block, reflecting degree of insulation. On wet blocks, when [T0-T3] is positive, skin surface is cooler than block, as a result of rate of evaporative cooling combined with insulation properties. Note the background in the pictures is [T2], the saturated water pad, always the coolest part of the picture, showing maximum rates of evaporative cooling from the warm block (measured as a TEWL rate of >300 g/m^2/h). **A.** DGAT1 KO; **B.** SKO; **C.** Sdc1KO; **D.** obese A^y mice; n $\geq$ 3 mice per assay. Data are expressed as mean $\pm$ SEM. Statistical analysis was performed with unpaired 2-tailed *t* test (****$P < 0.0001$; *$P < 0.05$; ns = not significant).

external biome [7]. Heparan sulfate itself was implicated as a modifier of sebaceous gland morphogenesis, using a conditional KO of Ext1, a key enzyme for heparan sulfate morphogenesis [14].

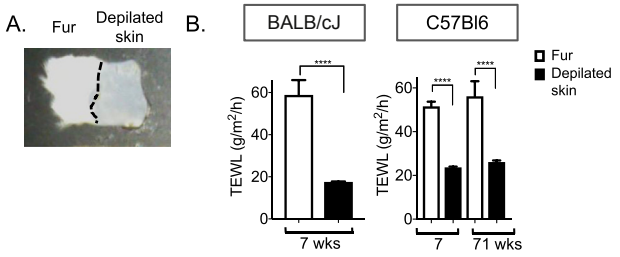

Figure 6: Fur increases transpiration rates. BALB/cJ mice pelts, depilated or not (**A**), or C57Bl6 pelts from mice at 7 and 71 weeks of age (similarly prepared), were analyzed for their rates of TEWL (n = 3, n = 5, n = 5, respectively**; B**). Data are expressed as mean $\pm$ SEM. Statistical analysis was performed with unpaired 2-tailed *t* test (****$P < 0.0001$).

We speculate that in addition to the gross changes of dWAT, sebaceous gland function may also be affected in Sdc1KO mice. For mice with a deficient epidermal barrier (SKO and DGAT1 KO), considerable energy is lost to evaporative cooling (Figure 10). These mice are cold-intolerant and susceptible to torpor (Table 1). Because their fur is thicker the phenotype of the DGAT1KO mice is less severe than the SKO mice; they show a 50% increase in evaporative cooling compared to the 100% increase demonstrated for SKO mice. Both of these mouse strains are highly resistant to diet-induced obesity; in other words, for mice with "metabolically inefficient" skins, we propose that the pathway to reserving calories as fat is suppressed. We speculate that a sensory function is activated in permeable skins that cool easily by water loss, inhibiting accumulation of fat.

Obese mice (thick dWAT) show decreased evaporative cooling; since there is little change in food intake or respiratory energy expenditure, the energy saved implies the anabolic demands of fat accumulation. These mice are known to be susceptible to cancer (Table 1).

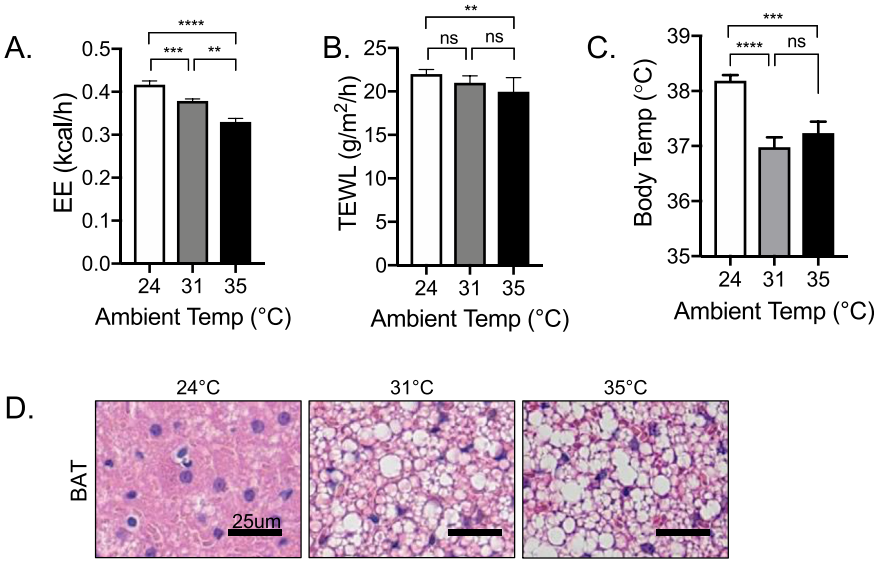

Figure 7: Thermogenic profiling of hairless SKH1 mice. **A.** EE was measured for mice housed at the temperatures indicated for >48 h (24 and 31 °C) or 24 h (35 °C) (n = 8). **B, C.** TEWL and rectal body temperatures were also measured for these mice. Data are expressed as mean ± SEM, and statistical analysis was performed with unpaired 2-tailed *t* tests (****$P < 0.0001$; ***$P < 0.001$; **$P < 0.01$; ns = not significant). **D.** Representative images show the dynamic range of lipid storage in BAT in mice housed at different ambient temperatures, as assayed by histological analysis (n = 8).

3.3. Evaporative cooling is affected by feeding regimens, including every-other-day feeding

Studies suggest that the rate of cooling by trans-epidermal water loss can be regulated not only by genetic variation of lipid production but also by environmental factors, including diet. For example, a dietary protocol called every-other-day feeding is known to confer considerable health benefit; mice on this protocol show much increased rates of trans-epidermal water loss [52]. Given our results, we suggest that increased evaporative cooling could be an effector of this protocol. Every-other-day feeding is a calorie restriction protocol that has many known health benefits, including lower cancer incidence [9,32]. Indeed, one of the benefits of calorie restriction protocols, whatever the species, are dramatically decreased rates of tumor development [30].

3.4. Two lipid lamellae, separated by a vascular bed, can provide precise heat transfer rates

DWAT and the epidermal barrier are separated by a highly vascularized dermal bed. Regulated major blood vessels deliver blood to this layer when the mouse is over-heated; in room temperature housing (sub-thermoneutral), the volume of blood in this layer is minimized, therefore all these tissue layers are likely to be well below core body temperature. The importance of dWAT and the epidermal barrier likely differ depending upon the ambient temperature. Note that both obesity and the Sdc1KO mutation may affect not only dWAT but also the lipids associated with the epidermal layer. Indeed, increased amounts and changes of composition of epidermal lipids have been described for obese human subjects [55]. Likewise, if SKO mice are pre-conditioned with a high fat diet, they show increased lipid content in their epidermal barrier and decreased susceptibility to hypothermia [41]. Obese mice, with less ability to lose heat through their skin, have been reported to drop their body temperature and resort to vasodilation of blood vessels in their tails [19]. We speculate that high fat diets may reduce evaporative loss through skin, promoting alternate fates for calorie deposition such as fat accumulation.

3.5. Evaporative cooling is high in high-density caging conditions

These data describe trans-epidermal water loss, which comprises only a fraction of the total water loss of the mammalian body: the energy losses we describe are therefore under-estimates. Total evaporative loss will include respiratory water vapor and, for human subjects, will also include more specialized water loss mechanisms such as sweating. The energy lost to evaporative cooling is determined as much by ambient humidity and windspeed as absolute temperature (other radiative and conductive losses depend upon the temperature gradient). Both these factors are worth consideration in our typical mouse housing conditions; firstly, humidity is not routinely controlled but can be sensed by mice. For example, mouse skin will adapt to dry environmental conditions by increasing the speed of regeneration of the epidermal permeability barrier [44]. Secondly, for typical "high-density" mouse housing the rate of air exchange is 60 cage volumes per hour, 1 per minute, which promotes high rates of cooling, beyond the usual sub-thermoneutral housing temperatures [23]. In these conditions, mouse number per cage, bedding, and igloos will have a major effect on results of metabolism-dependent assays.

3.6. Surface temperatures measured by FLIR cameras can be misleading

Evaporative cooling and insulation both lower surface temperatures with exactly opposite metabolic effect: evaporative cooling is an energy loss, where insulation conserves energy. FLIR assays are likely to be especially inaccurate for surfaces that are already wet, like eyes [17]. The warmer the blood, the higher the rate of evaporative cooling, the lower the surface temperature. Our current study illustrates how misleading infrared thermographic assessment of surface temperatures can be for gauging metabolic activity and insulation. Surface temperatures of live mice cannot be used directly as a measure of insulation, since heat production is adjusted to maintain homeostasis [34]. Infrared thermographic imaging of the whole body can however identify shifting sources of heat production, for example a switch from interscapular BAT to the more widely disseminated pattern of ventral beige depots [17].

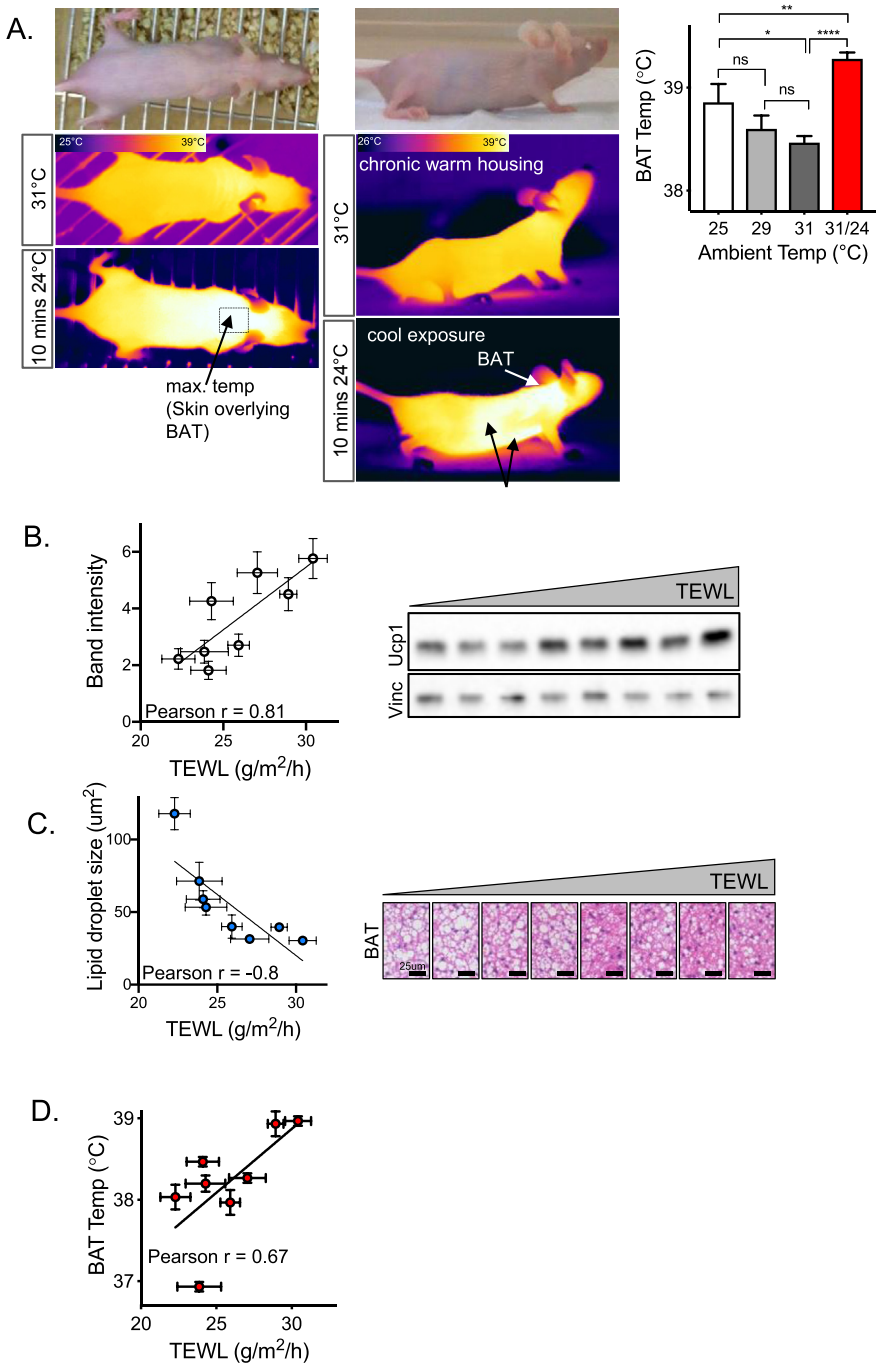

Figure 8: Thermogenic activity is increased in mice that show high rates of evaporative cooling. A. Live imaging of thermogenic activity. Representative images show a hairless SKH1 female mouse housed at warm temperature (31 °C, for >1 week) and after a minor cool exposure (room temperature 24 °C, for 10 min). Side views show percolation of warmed blood throughout the internal organs, possibly also revealing autonomous heat sources (indicated with arrows). Maximum temperatures were visualized over BAT depot (interscapular area) and quantified for different ambient housing temperatures (equilibrated for >4 h; n = 8), and for mice after cool exposure (31/24; 31 °C–24 °C for 10 min; n = 8; right hand side). Thermographic images were analyzed by FLIR software; a box drop was used to measure the maximum temperature of a region of interest, expressed as the mean ± SEM and analyzed using an unpaired 2-tailed *t* test (****$P < 0.0001$; **$P < 0.01$; *$P < 0.05$; ns = not significant). **B–D. Correlating BAT activation with high rates of evaporative cooling.** TEWL and BAT activation were measured for 8 SKH1 female mice (14–18 weeks of age), housed at 31 °C, using a molecular marker (UCP1 protein signal from Western blotting of BAT; **B**), a histological marker (relative area of lipid droplets in BAT; **C**) and live imaging of surface temperature of BAT (FLIR; **D**). Increasing TEWL was significantly correlated with increasing UCP1 protein (**B**; p = 0.013) and decreasing BAT lipid content (**C**; p = 0.017), trending towards significance with respect to live BAT temperature (**D**; p = 0.06). Individual mice (n = 8) are represented by the data points on **B–D** (shown as mean ± SD), and correlation analysis was performed to generate r values, the Pearson correlation coefficient.

Table 2 — Comparison of alterations of power chain for test mouse strains (calories consumed, energy expenditure and evaporative cooling). Figures for food consumption/EE are taken from the publications indicated, and calculations are provided in detail in Table S1.

	Change of food consumption	Change of energy expenditure [kcal/h/kg] compared to control ΔEE [W/mouse]	Change of evaporative cooling [g/m^2/h] [W] (this study)	Source energy expenditure calculations
DGAT1 KO	No change	Increased 22% Δ+4.17 kcal/h/kg **Δ0.125 W**	DKO 31.0 Control 20.2 Increased 53.4% **Δ + 0.076W**	[47,53]
SKO	Increase of 100% (3.74 g/day) **Δ0.60 W**	SKO 46.2 control 31.2 Increased 48% Δ+15 kcal/h/kg **Δ0.45 W**	SKO 49.5 Control 23.7 Increased 108.8% **Δ + 0.18W**	[41]
Obese A^y	No change	Obese 15.20 control 15.54 Decreased by 2.2% Δ-0.34 kcal/h/kg **Δ − 0.01 W**	Obese 17.01 control 23.4 Decreased 10.3% **Δ − 0.016W**	[40]
Sdc1 KO	Increase of 6.7% (0.24 g/day) **Δ + 0.04 W**	Sdc1KO 21.01 control 18.13 Increased 15% Δ+2.9 kcal/h/kg **Δ0.09 W**	Sdc1KO 33.7 control 22.5 Increased 49.7% **Δ + 0.078W**	[25]

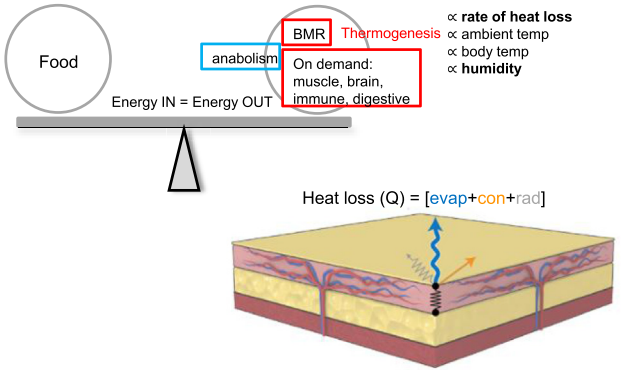

Figure 9: Summary diagram of energy balance. At homeostasis, energy expenditures equal the incoming calories contained in food, plus short-term mobilization of stored calories. Expenditures include the basal metabolic rate (BMR), together with anabolism (including cell growth of renewing lineages and deposition of glycogen and fat), and "on-demand" processes such as neural function, motor activity, immune defenses and digestion. All these processes, except anabolism, generate heat (indicated by red boxes for heat generation, blue for endothermy). If this does not maintain body temperature at sub-thermoneutral temperatures, (non-shivering) thermogenesis is activated. The rate of heat generation required depends upon the factors indicated, the ambient temperature (including wind speed and humidity), the body temperature set-point, and the rate of heat loss, determined by animal behavior, and the properties of their body coverings, including the skin. The illustration of skin shows the biophysical processes that govern heat loss (Q), taken from Figure 2, a combination of evaporation, convection and radiation.

3.7. Direct assay of evaporative cooling and other modes of heat loss can avoid the shortcomings of using total energy expenditure for interpretation of whole-body phenotypes

A published study suggested there was no insulating effect of obesity in various mouse models [18]; our results suggest that increased fat associated with skin could conserve energy via decreased evaporative cooling. By way of resolution of these opposite conclusions, Fischer et al. did not measure the properties of skin directly but inferred the relative insulation from plotting energy expenditure against a range of sub-thermoneutral temperatures for different strains of mice. Since energy expenditure is the total of all respiratory loads (Figure 9), it is a complex sum, geared towards homeostasis. It includes activity, behavior, shivering, basal metabolic rates (with heartbeat), alongside the chemical thermogenic response and novel, non-UCP1-dependent responses, (with uncertain respiratory stoichiometry) [22,26]. As ambient temperature decreases, the animal may trigger specific responses, with various effects on energy expenditure; for example, some may run and become hyperactive while others may tend towards torpor or show decreased body temperature. These have different impacts on O_2 consumption, one showing dramatically increased O_2 consumption at lower temperatures, and the other much less. Neither specifically implicates different insulation. Indeed, we suggest that any single factor, such as insulation, cannot be deduced from Scholander plots, which reflect instead the total energetic response of the mouse to cool exposure.

3.8. Conclusions and implications

We have drawn attention to the energy loss represented by trans-epidermal water loss and suggest that this could be an important regulator of calorie disposition in mammals. Our methods quantify the properties of skin as they impact studies of obesity, diabetes and other diseases. By altering ambient humidity or by adjusting trans-epidermal water loss with topical applications, it will be possible to establish the impact of this heat loss on physiology. Human skin is different from mouse skin: it consists of a relatively thick layer of skin-associated fat of different etiology and composition. It averages 6.3 and 10.0 mm for men and women respectively (Kasza et al., unpublished). Human trans-epidermal water loss is known to be highly regulated, but the extent that an individual's skin can direct their metabolism and susceptibility to obesity and metabolic disease is not yet known. We suggest that trans-epidermal water loss be assayed routinely to assess the correlation between this parameter and metabolic disease susceptibility. Given that the skin is the most accessible and therefore druggable organ in the mammalian body, its potential for modifying health outcomes waits to be tapped.

4. MATERIALS AND METHODS

4.1. Mouse strains, mouse housing and ethics statement

We used five different types of female mice for this study (more strain-specific information is summarized in Table 1): 1) Agouti lethal yellow (**A^y**/a; C57Bl/6J) mice (Jackson labs stock#002468) are obese due to over-expression of the agouti peptide in the brain. This peptide is an

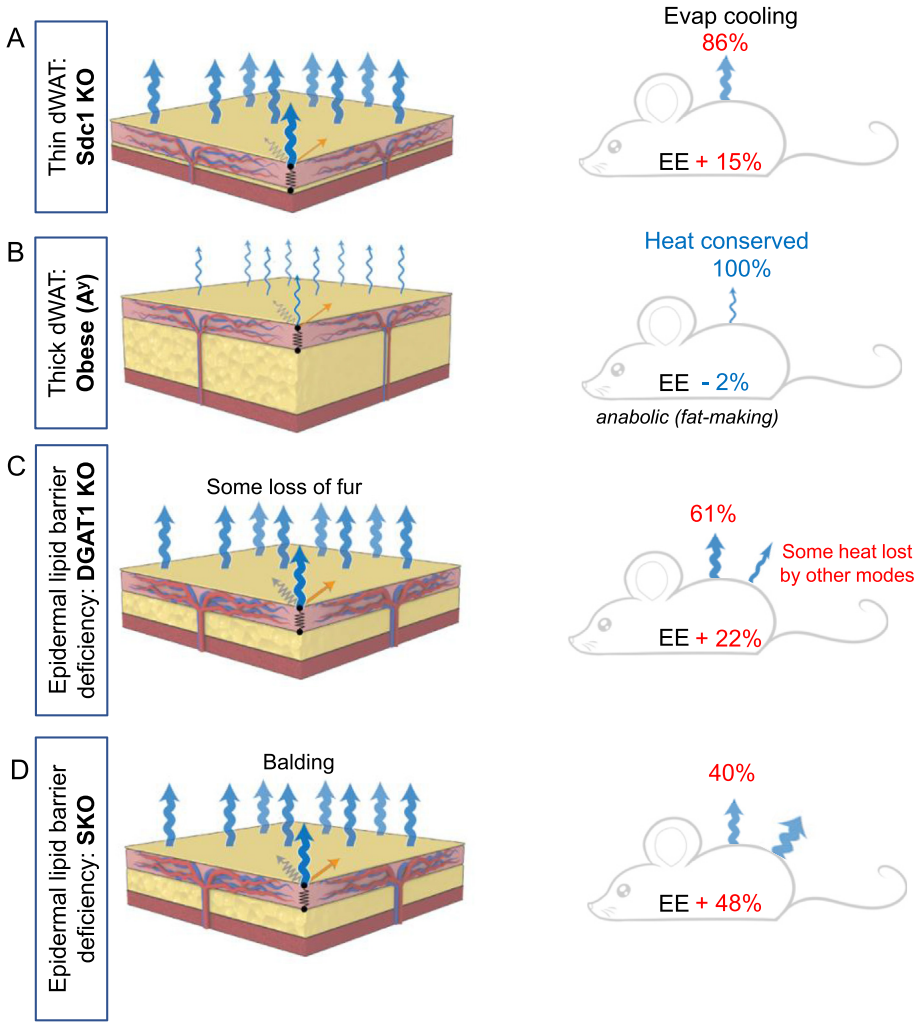

Figure 10: Summary schemes of the effect of deficient skin lipid lamellae on evaporative cooling and energy balance. On the left are summary images of the skins evaluated by this study, illustrating the heat losses from each type of skin by evaporative cooling. On the right are schemes that show the calculated energy flow through the system, taken from Table 2 and Table S1. For each strain, the changes in energy expenditure (EE) are calculated and expressed as a % difference compared to control. The power lost to evaporative cooling is expressed as a proportion (%) of change of EE, where increases are shown in red, and decreases are shown in blue. Thus for mice with normal hair (such as Sdc1 KO), increased evaporative cooling accounts for the majority of increased energy expenditure (86%); for strains that lose their hair, evaporative cooling accounts for approximately half of the increased metabolic rate, the rest probably reflects radiative losses.

antagonist of the melanocortin4 receptor (MC4R), and leads to hyperphagia (over-eating), hypoactivity and increased fat mass [11,40]. 2) Syndecan-1 knockout mice (**Sdc1KO**) have a constitutive loss of expression of the heparin sulfate proteoglycan, syndecan1. These mice show thin dWAT and are cold-stressed; they are also tumor resistant [25,33]. 3) **SKO** mice with a mutation of the lipid metabolism enzyme, stearoyl-coenzymeA desaturase (SCD1) directed to the basal layer of epithelial tissues such as skin (using a conditional SCD1 flox allele and a keratin 14 (K14)-cre driver) [41]. This enzyme catalyzes a key step of a metabolic pathway that converts saturated fatty acids (palmitate and stearate) into monounsaturated fatty acids (palmitoleate and oleate) [43]. SKO mice are resistant to diet-induced obesity and show deficiencies of most skin-associated ceramides [35,43]. 4) **DGAT1 KO** mice have a mutation in the acyl CoA:diacylglycerol transferase enzyme responsible for the synthesis of triglycerides; they are lean and resistant to diet-induced obesity and show deficient epidermal ceramide synthesis [47]. 5) SKH1-Elite (abbreviated SKH1 mice; Charles River; stock#477; Crl:SKH1-*Hr*^{hr}) are immunocompetent but hairless outbred strain of mice, that are used for dermatological studies for their established correspondence to some of the properties of human skin [5].

These studies were performed in strict accordance with the recommendations in the Guide for the Care and Use of Laboratory Animals of the National Institutes of Health. Experimental protocols were approved by the University of Wisconsin School of Medicine and Public Health Animal Care and Use Committee. The number of mice used to perform this study was minimized, and every effort was made to reduce the chance of pain or suffering.

Mice were maintained on a 12 h light and dark cycle with free access to water and chow diet Teklad#8604, Harlan Laboratories, Madison WI. To assay skin properties, mice were anesthetized, depilated using Nair, and rinsed the day before euthanasia; mice were allowed to recover on a warming pad, before being housed overnight in cages with igloos. SKH1 female mice were singly housed in controlled environments (indicated temperature at 20% humidity for the periods of

time described) for the purpose of evaluating skin properties and BAT activation by FLIR and TEWL.

4.2. Metabolic cage measurements

For individual assay of multiple metabolic parameters (O_2, CO_2, food and water consumption), SKH1-Elite mice were individually caged and housed in a LabMaster modular animal monitoring system from TSE Systems (Chesterfield, MO), acclimated for the indicated period of time at 24 °C, 31 °C or 35 °C, and monitored daily. A Thermalert TH-5 monitoring thermometer with a RET-3 mouse rectal probe was used to monitor body temperature. Body composition measurement of fat, lean, free water and total water masses were delivered by EchoMRI analyzer before and after the metabolic cage studies.

4.3. Tissue collection and molecular and histological analysis

Interscapular BAT, other tissues and skin were dissected and paraformaldehyde fixed (4%) overnight before paraffin embedding and sectioning/staining. For quantification of lipid droplet size, dermal white adipose tissue (dWAT) thickness and density of vessels stained by podocalyxin (PdcX), six independent fields were obtained for each tissue from each mouse and quantified using open source Fiji image processing package (https://loci.wisc.edu/software/fiji). BAT tissue samples were promptly dissected and flash frozen for lysis and analysis of UCP1 expression via immunoblotting as described by Kasza et al. [25], using anti-UCP1 antibody (cat#ab10983) from Abcam.

4.4. Infrared thermography and trans-epidermal water loss assay

To measure surface temperatures by infrared thermography, we used a hand-held FLIR T360 camera (FLIR Systems, Oregon). The following experimental controls were performed: the infrared emissivity of the dry block, and the block covered with a full thickness wet pad, was >98% and consistent across the whole surface. For live imaging of thermogenic activity, mice were placed on the cage wire and restrained by the tail. For quantification of skin surface temperature above interscapular BAT, three independent images were obtained for each mouse. All thermographic images were quantified using FLIR Tools Advanced Thermal Analysis and Reporting software. Assays of skins from euthanized mice were complete in less than 10 min; these skins were transferred quickly from dry to wet block. On the wet block, their properties remained stable and intact *ex vivo* for several hours (both by FLIR and TEWL imaging). The FLIR camera was mounted on a dark plastic crate containing the test block and samples, to eliminate environmental contributions of lights, operator reflections, and air conditioning vents for this heat-sensitive assay. Samples were compared (pairwise) on the same block at the same time in the same environmental conditions. A humidity probe (Delfintech) was included inside the crate, and little change was observed during the course of photography. For imaging, the skin is dissected to exclude subcutaneous mammary gland before application to warm block. Pin drops in the software of the FLIR camera are used to record surface temperatures; each photograph is internally and externally calibrated to show actual temperatures; anagen stage patches (including dense hair follicles, see arrows pointing to examples on skins of Figure 5C) and edge effects are excluded from the analysis.

We used a Vapometer (Delfintech) hand-held probe to assess trans-epidermal water loss (TEWL); a picture is shown in Figure 2D. This is a closed chamber instrument with a rubber gasket, laid gently onto the surface of interest. Inside the chamber is a calibrated humidity sensor that reads out evaporation rates as g/m^2/h. The chamber is sequestered during the measurement period and unaffected by ambient airflows. Live measurements were taken from the abdominal flank of mice restrained gently by the tail; most female mice (and notably SKH1 mice) were calm during this procedure, which last between 8 and 20 s. Anesthesia by inhalants reduces body and skin temperatures within minutes and are to be avoided for this purpose. The relative magnitude of water loss measured by TEWL was verified by weight of evaporative losses over the course of 2–3 h. At least 5 separate TEWL measurements were made per pelt. Control and test samples were compared on the same block, in batches of 4, to test for day-to-day changes of performance.

4.5. Immunofluorescent staining of mouse tissue

Immunofluorescent staining on podocalyxin (PdcX), perilipin (PLN) and smooth muscle actin (SMA) and expression was performed as described in detail by Kasza et al. (Kasza et al., 2014). Briefly, tissues were deparaffinized, re-hydrated, and processed for heat-induced epitope retrieval. After blocking, samples were incubated overnight with the primary antibody, and the secondary antibodies for 1 h. Samples were rinsed and incubated with conjugated antibodies for 1 h, then visualized on a confocal microscope (Nikon A1RS Confocal Microscope). The catalog numbers of the antibodies are as follows: podocalyxin (AF1556, R&D Systems), perilipin–Alexa Fluor647 conjugate (NB110-40760AF647, Novus Biologicals), SMA-FITC conjugate (F3777, Sigma-Aldrich), donkey anti-goat Alexa Fluor 546 (A11056, Thermo Fisher Scientific). Normal goat serum for blocking was obtained from Jackson ImmunoResearch Laboratories, and ProLong Gold Antifade Reagent with DAPI for nuclear staining was from Invitrogen.

4.6. Statistics

Data are expressed as mean ± SEM. Statistical analysis was performed with unpaired 2-tailed *t* tests. For correlation analysis Pearson correlation coefficient was calculated. All studies were plotted using GraphPrism8 software. *P* values less than 0.05 were considered statistically significant. $^{****}P < 0.0001$; $^{***}P < 0.001$; $^{**}P < 0.01$; $^{*}P < 0.05$. Specific details for n values are noted in each figure legend.

ACKNOWLEDGEMENTS

We appreciate the expert histology assistance from Satoshi Kinoshita in the TRIP Lab (Department of Pathology), for assistance by the staff of the University of Wisconsin-Madison Biotron Laboratory environmentally controlled housing unit, for technical advice from Jouni Nuutinen at Delfin Technologies, Kuopio, Finland, and for the insight of Avtar Roopra (Department of Neuroscience) and Bob Holz (Space Science and Engineering Center, UW). Research reported in this publication was supported by NIGMS RO1GM113142 (CMA), RO1 DK62876 (OAM), R24 DK092759 (OAM), and the National Institute of Arthritis and Musculoskeletal and Skin Diseases of the National Institutes of Health (NIH) under Award Number P30 AR066524, Skin Diseases Research Center at the University of Wisconsin, pilot award MSN169122 (IK).

ABBREVIATIONS

BAT	brown adipose tissue;
scWAT	subcutaneous white adipose tissue
iWAT	inguinal white adipose tissue for mice
vWAT	visceral white adipose tissue
TEWL	trans-epidermal water loss
FLIR	forward looking infrared thermography
EE	energy expenditure

CONFLICT OF INTEREST

The authors declare no conflicts of interest.

APPENDIX A. SUPPLEMENTARY DATA

Supplementary data to this article can be found online at https://doi.org/10.1016/j.molmet.2019.06.023.

REFERENCES

[1] Alexander, C.M., Kasza, I., Yen, C.L., Reeder, S.B., Hernando, D., Gallo, R.L., et al., 2015. Dermal white adipose tissue: a new component of the thermogenic response. The Journal of Lipid Research 56(11):2061–2069.

[2] Azzi, L., El-Alfy, M., Martel, C., Labrie, F., 2005. Gender differences in mouse skin morphology and specific effects of sex steroids and dehydroepiandrosterone. Journal of Investigative Dermatology 124(1):22–27.

[3] Bartelt, A., Heeren, J., 2012. The holy grail of metabolic disease: brown adipose tissue. Current Opinion in Lipidology 23(3):190–195.

[4] Bartelt, A., Heeren, J., 2014. Adipose tissue browning and metabolic health. Nature Reviews Endocrinology 10(1):24–36.

[5] Benavides, F., Oberyszyn, T.M., VanBuskirk, A.M., Reeve, V.E., Kusewitt, D.F., 2009. The hairless mouse in skin research. Journal of Dermatological Science 53(1):10–18.

[6] Binczek, E., Jenke, B., Holz, B., Gunter, R.H., Thevis, M., Stoffel, W., 2007. Obesity resistance of the stearoyl-CoA desaturase-deficient (scd1-/-) mouse results from disruption of the epidermal lipid barrier and adaptive thermoregulation. Biological Chemistry 388(4):405–418.

[7] Bode, L., Salvestrini, C., Park, P.W., Li, J.P., Esko, J.D., Yamaguchi, Y., et al., 2008. Heparan sulfate and syndecan-1 are essential in maintaining murine and human intestinal epithelial barrier function. Journal of Clinical Investigation 118(1):229–238.

[8] Boiten, W.A., Berkers, T., Absalah, S., van Smeden, J., Lavrijsen, A.P.M., Bouwstra, J.A., 2018. Applying a vernix caseosa based formulation accelerates skin barrier repair by modulating lipid biosynthesis. The Journal of Lipid Research 59(2):250–260.

[9] Brandhorst, S., Choi, I.Y., Wei, M., Cheng, C.W., Sedrakyan, S., Navarrete, G., et al., 2015. A periodic diet that mimics fasting promotes multi-system regeneration, enhanced cognitive performance, and healthspan. Cell Metabolism 22(1):86–99.

[10] Cannon, B., Nedergaard, J., 2009. Thermogenesis challenges the adipostat hypothesis for body-weight control. Proceedings of the Nutrition Society 68(4):401–407.

[11] Carroll, L., Voisey, J., van Daal, A., 2004. Mouse models of obesity. Clinics in Dermatology 22(4):345–349.

[12] Chen, H.C., Smith, S.J., Tow, B., Elias, P.M., Farese Jr., R.V., 2002. Leptin modulates the effects of acyl CoA: diacylglycerol acyltransferase deficiency on murine Fur and sebaceous glands. Journal of Clinical Investigation 109(2):175–181.

[13] Chuong, C.M., Nickoloff, B.J., Elias, P.M., Goldsmith, L.A., Macher, E., Maderson, P.A., et al., 2002. What is the 'true' function of skin? Experimental Dermatology 11(2):159–187.

[14] Coulson-Thomas, V.J., Gesteira, T.F., Esko, J., Kao, W., 2014. Heparan sulfate regulates hair follicle and sebaceous gland morphogenesis and homeostasis. Journal of Biological Chemistry 289(36):25211–25226.

[15] David Boothe, W., Tarbox, J.A., Tarbox, M.B., 2017. Atopic dermatitis: pathophysiology. Advances in Experimental Medicine & Biology 1027:21–37.

[16] Elattar, S., Satyanarayana, A., 2015. Can Brown fat win the battle against white fat? Journal of Cellular Physiology 230(10):2311–2317.

[17] Fabbiano, S., Suarez-Zamorano, N., Rigo, D., Veyrat-Durebex, C., Stevanovic Dokic, A., Colin, D.J., et al., 2016. Caloric restriction leads to browning of white adipose tissue through type 2 immune signaling. Cell Metabolism 24(3):434–446.

[18] Fischer, A.W., Csikasz, R., von Essen, G., Cannon, B., Nedergaard, J., 2016. No insulating effect of obesity. American Journal of Physiology. Endocrinology and Metabolism ajpendo 00093 02016.

[19] Fischer, A.W., Hoefig, C.S., Abreu-Vieira, G., de Jong, J.M., Petrovic, N., Mittag, J., et al., 2016. Leptin raises defended body temperature without activating thermogenesis. Cell Reports 14(7):1621–1631.

[20] Harms, M., Seale, P., 2013. Brown and beige fat: development, function and therapeutic potential. Nature Medicine 19(10):1252–1263.

[21] Hazama, Y., Maekawa, T., Miki, R., Oshima, S., Egawa, Y., Morimoto, K., et al., 2016. Effect of physiological changes in the skin on systemic absorption of tacrolimus following topical application in rats. Biological and Pharmaceutical Bulletin 39(3):343–352.

[22] Ikeda, K., Kang, Q., Yoneshiro, T., Camporez, J.P., Maki, H., Homma, M., et al., 2017. UCP1-independent signaling involving SERCA2b-mediated calcium cycling regulates beige fat thermogenesis and systemic glucose homeostasis. Nature Medicine 23(12):1454–1465.

[23] Karp, C.L., 2012. Unstressing intemperate models: how cold stress undermines mouse modeling. Journal of Experimental Medicine 209(6):1069–1074.

[24] Kasza, I., Hernando, D., Roldan-Alzate, A., Alexander, C.M., Reeder, S.B., 2016. Thermogenic profiling using magnetic resonance imaging of dermal and other adipose tissues. JCI Insight 1(13):e87146.

[25] Kasza, I., Suh, Y., Wollny, D., Clark, R.J., Roopra, A., Colman, R.J., et al., 2014. Syndecan-1 is required to maintain intradermal fat and prevent cold stress. PLoS Genetics 10(8):e1004514.

[26] Kazak, L., Chouchani, E.T., Jedrychowski, M.P., Erickson, B.K., Shinoda, K., Cohen, P., et al., 2015. A creatine-driven substrate cycle enhances energy expenditure and thermogenesis in beige fat. Cell 163(3):643–655.

[27] Kazak, L., Chouchani, E.T., Lu, G.Z., Jedrychowski, M.P., Bare, C.J., Mina, A.I., et al., 2017. Genetic depletion of adipocyte creatine metabolism inhibits diet-induced thermogenesis and drives obesity. Cell Metabolism 26(4):693.

[28] Kruse, V., Neess, D., Faergeman, N.J., 2017. The significance of epidermal lipid metabolism in whole-body physiology. Trends in Endocrinology and Metabolism 28(9):669–683.

[29] Lee, Y.H., Kim, S.N., Kwon, H.J., Granneman, J.G., 2017. Metabolic heterogeneity of activated beige/brite adipocytes in inguinal adipose tissue. Scientific Reports 7:39794.

[30] Longo, V.D., Fontana, L., 2010. Calorie restriction and cancer prevention: metabolic and molecular mechanisms. Trends in Pharmacological Sciences 31(2):89–98.

[31] Madison, K.C., 2003. Barrier function of the skin: "la raison d'etre" of the epidermis. Journal of Investigative Dermatology 121(2):231–241.

[32] Mattson, M.P., Longo, V.D., Harvie, M., 2017. Impact of intermittent fasting on health and disease processes. Ageing Research Reviews 39:46–58.

[33] McDermott, S.P., Ranheim, E.A., Leatherberry, V.S., Khwaja, S.S., Klos, K.S., Alexander, C.M., 2007. Juvenile syndecan-1 null mice are protected from carcinogen-induced tumor development. Oncogene 26(10):1407–1416.

[34] Meyer, C.W., Ootsuka, Y., Romanovsky, A.A., 2017. Body temperature measurements for metabolic phenotyping in mice. Frontiers in Physiology 8:520.

[35] Miyazaki, M., Sampath, H., Liu, X., Flowers, M.T., Chu, K., Dobrzyn, A., et al., 2009. Stearoyl-CoA desaturase-1 deficiency attenuates obesity and insulin resistance in leptin-resistant obese mice. Biochemical and Biophysical Research Communications 380(4):818–822.

[36] Natsuga, K., 2014. Epidermal barriers. Cold Spring Harbor Perspectives in Medicine 4(4):a018218.

[37] Ndiaye, M.A., Nihal, M., Wood, G.S., Ahmad, N., 2014. Skin, reactive oxygen species, and circadian clocks. Antioxidants and Redox Signaling 20(18):2982–2996.

[38] Nedergaard, J., Cannon, B., 2014. The browning of white adipose tissue: some burning issues. Cell Metabolism 20(3):396–407.

[39] Neess, D., Bek, S., Bloksgaard, M., Marcher, A.B., Faergeman, N.J., Mandrup, S., 2013. Delayed hepatic adaptation to weaning in ACBP-/- mice is caused by disruption of the epidermal barrier. Cell Reports 5(5):1403–1412.

[40] Nelson, D.W., Gao, Y., Spencer, N.M., Banh, T., Yen, C.L., 2011. Deficiency of MGAT2 increases energy expenditure without high-fat feeding and protects

genetically obese mice from excessive weight gain. The Journal of Lipid Research 52(9):1723—1732.

[41] Sampath, H., Flowers, M.T., Liu, X., Paton, C.M., Sullivan, R., Chu, K., et al., 2009. Skin-specific deletion of stearoyl-CoA desaturase-1 alters skin lipid composition and protects mice from high fat diet-induced obesity. Journal of Biological Chemistry 284(30):19961—19973.

[42] Sampath, H., Ntambi, J.M., 2011. The role of stearoyl-CoA desaturase in obesity, insulin resistance, and inflammation. Annals of the New York Academy of Sciences 1243:47—53.

[43] Sampath, H., Ntambi, J.M., 2014. Role of stearoyl-CoA desaturase-1 in skin integrity and whole body energy balance. Journal of Biological Chemistry 289(5):2482—2488.

[44] Sato, J., Denda, M., Chang, S., Elias, P.M., Feingold, K.R., 2002. Abrupt decreases in environmental humidity induce abnormalities in permeability barrier homeostasis. Journal of Investigative Dermatology 119(4):900—904.

[45] Schreiber, R., Diwoky, C., Schoiswohl, G., Feiler, U., Wongsiriroj, N., Abdellatif, M., et al., 2017. Cold-induced thermogenesis depends on ATGL-mediated lipolysis in cardiac muscle, but not Brown adipose tissue. Cell Metabolism 26(5):753—763 e757.

[46] Shih, M.Y., Kane, M.A., Zhou, P., Yen, C.L., Streeper, R.S., Napoli, J.L., et al., 2009. Retinol esterification by DGAT1 is essential for retinoid homeostasis in murine skin. Journal of Biological Chemistry 284(7):4292—4299.

[47] Smith, S.J., Cases, S., Jensen, D.R., Chen, H.C., Sande, E., Tow, B., et al., 2000. Obesity resistance and multiple mechanisms of triglyceride synthesis in mice lacking Dgat. Nature Genetics 25(1):87—90.

[48] Speakman, J.R., Keijer, J., 2012. Not so hot: optimal housing temperatures for mice to mimic the thermal environment of humans. Molecular Metabolism 2(1):5—9.

[49] Stanford, K.I., Bishop, J.R., Foley, E.M., Gonzales, J.C., Niesman, I.R., Witztum, J.L., et al., 2009. Syndecan-1 is the primary heparan sulfate proteoglycan mediating hepatic clearance of triglyceride-rich lipoproteins in mice. Journal of Clinical Investigation 119(11):3236—3245.

[50] Sundberg, J.P., Boggess, D., Sundberg, B.A., Eilertsen, K., Parimoo, S., Filippi, M., et al., 2000. Asebia-2J (Scd1(ab2J)): a new allele and a model for scarring alopecia. American Journal Of Pathology 156(6):2067—2075.

[51] Sundberg, J.P., Silva, K.A., 2012. What color is the skin of a mouse? Veterinary Pathology 49(1):142—145.

[52] Xie, K., Neff, F., Markert, A., Rozman, J., Aguilar-Pimentel, J.A., Amarie, O.V., et al., 2017. Every-other-day feeding extends lifespan but fails to delay many symptoms of aging in mice. Nature Communications 8(1):155.

[53] Yen, C.L., Stone, S.J., Koliwad, S., Harris, C., Farese Jr., R.V., 2008. Thematic review series: glycerolipids. DGAT enzymes and triacylglycerol biosynthesis. The Journal of Lipid Research 49(11):2283—2301.

[54] Yen, T.T., Gill, A.M., Frigeri, L.G., Barsh, G.S., Wolff, G.L., 1994. Obesity, diabetes, and neoplasia in yellow A(vy)/- mice: ectopic expression of the agouti gene. The FASEB Journal 8(8):479—488.

[55] Yosipovitch, G., DeVore, A., Dawn, A., 2007. Obesity and the skin: skin physiology and skin manifestations of obesity. Journal of the American Academy of Dermatology 56(6):901—916 quiz 917-920.

